Open Access Library Journal
2025, Volume 12, e13945
ISSN Online: 2333-9721
ISSN Print: 2333-9705

Gold Enrichment Patterns and Integrated Deep-Shallow Metallogenic Model of the Liaoshang Gold Deposit, Northeastern Margin of the Jiaolai Basin, China

Deping Li[1], Zhixin Wang[1], Jian Zou[1], Feng Hu[1], Junxi Yang[2], Jiangtao Shan[2]

[1]Department of Basic Geology, Shandong No. 3 Institute of Geology and Mineral Exploration, Yantai, China
[2]Liaoshang Gold Mine, Shandong Humon Smelting Co., Ltd., Yantai, China
Email: li_deping@foxmail.com

How to cite this paper: Li, D.P., Wang, Z.X., Zou, J., Hu, F., Yang, J.X. and Shan, J.T. (2025) Gold Enrichment Patterns and Integrated Deep-Shallow Metallogenic Model of the Liaoshang Gold Deposit, Northeastern Margin of the Jiaolai Basin, China. *Open Access Library Journal*, **12**: e13945.
https://doi.org/10.4236/oalib.1113945

Received: July 13, 2025
Accepted: August 4, 2025
Published: August 7, 2025

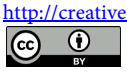

Abstract

The Liaoshang gold deposit in the Jiaolai Basin (North China Craton) has had its deep resource potential limited by inadequately understood vertical metallogenic patterns. Using 220 drill holes, 523 stope samples (38879.7 m), and 18,415 Au assays, this study employs implicit 3D modeling to decouple deep-shallow mineralization systems. A critical boundary at −400 m is identified: Shallow (<−400 m) NE-striking steep veins (avg. 1.2 m thick, Au > 5.5 g/t) are controlled by monzogranite-marble contacts, while deep (≥−400 m) stratiform orebodies (avg. 18.4 m thick, Au = 2.1 ± 0.8 g/t) follow the basin-margin detachment fault. Coefficient of variation analysis (shallow CV = 1.52 vs deep CV = 0.37) reveals a "deep pervasive alteration - shallow boiling enrichment" mechanism. Early-stage fluids formed disseminated mineralization via detachment-zone metasomatism; late-stage boiling at <−400 m triggered rapid gold precipitation into high-grade veins. The resulting 3D targeting model prioritizes silicified zones below −500 m.

Subject Areas

Mineral Exploration, Ore Geology

Keywords

Jiaolai Basin, Liaoshang Gold Deposit, 3D Modeling, Vertical Zonation, Metallogenic Dynamics, Exploration Targeting

1. Introduction

1.1. Regional Geological Setting

The Jiaolai Basin is situated on the southeastern margin of the North China Craton and constitutes a significant part of the Circum-Pacific metallogenic domain [1]. Since the Mesozoic, influenced by the subduction of the Paleo-Pacific Plate, the region has undergone intense extensional tectonics, forming a basin-and-range structural framework dominated by NE-trending faults [2] (**Figure 1**). This specific dynamic setting triggered large-scale magmatic-hydrothermal activity, making the Jiaodong region a globally rare giant gold province, with cumulative proven gold resources exceeding 5000 t [3]. Notably, recent exploration practices indicate that gold deposits in the Jiaodong region commonly exhibit significant vertical zonation—shallow levels are dominated by high-grade quartz vein and carbonate vein types, transitioning progressively to low-grade altered rock types at depth [4]. This characteristic is particularly pronounced at the Liaoshang gold deposit on the northeastern margin of the basin. With proven reserves exceeding 69 t, the genetic link between its deep and shallow mineralization remains inadequately understood.

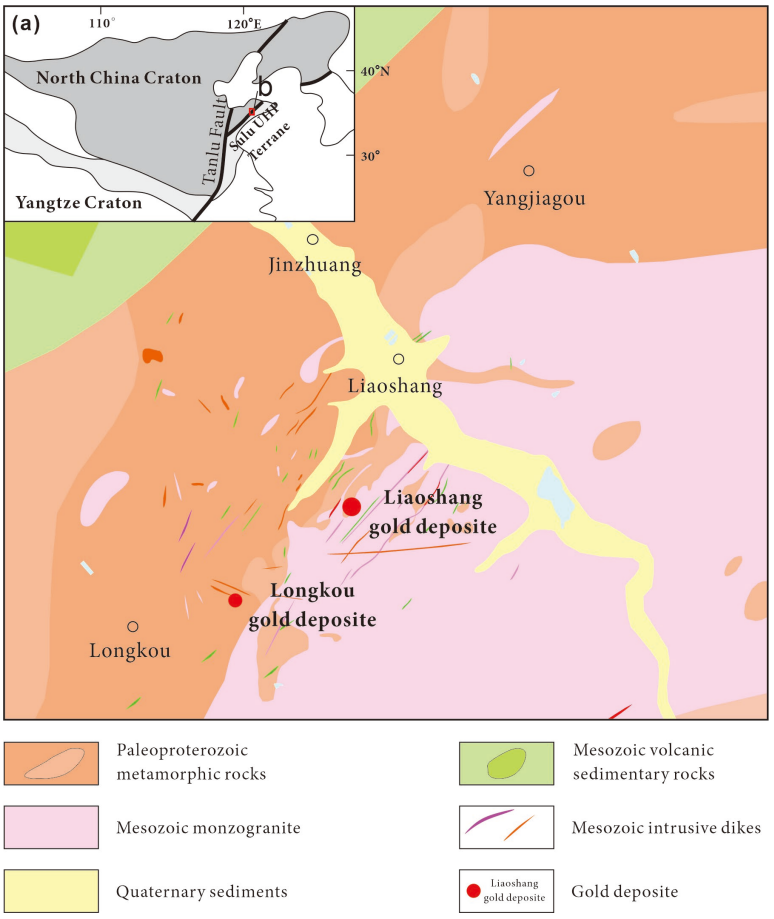

Figure 1. Simplified geological map of the Northeastern margin of the Jiaolai basin (adapted from *Liaoshang Exploration Rep.*, 2019).

1.2. Problems and Research Status

Previous research on the Liaoshang deposit has primarily focused on three aspects: 1) Structural controls on mineralization, emphasizing the ore-conducting role of NE-trending fault zones [5]; 2) Nature of ore-forming fluids, indicating mesothermal to epithermal, slightly alkaline hydrothermal solutions [6] [7]. Studies of fluid inclusions and H-O-C-S-Pb isotope geochemistry also show that the ore-forming fluids belong to a medium-low temperature, medium-low salinity, low-density, CO_2-rich, reduced hydrothermal system, likely a mixture of mantle-derived primary fluids and magmatic fluids + meteoric water [8] [9]; 3) Constraints on metallogenic age: Mineralogical and petrological studies, including mineral typomorphic characteristics, suggest a Mesozoic formation age for the deposit [9] [10]. Mineralization in the adjacent Longkou-Tudui gold district occurred at 120 ± 10 Ma within the NE-trending detachment system along the basin margin [11], and the nearby Qianchuiliu gold deposit formed between 128 - 116 Ma, representing part of the gold metallogeny in the northeastern Jiaolai Basin margin [12]. However, these studies have significant limitations: they predominantly rely on traditional 2D cross-section analysis, making it difficult to quantitatively characterize the 3D morphology variations of ore bodies, particularly lacking systematic analysis of the spatial coupling relationship between shallow high-grade vein-type ores and deep, large-tonnage low-grade ores. As noted by Groves [13]: "The vertical extent of orogenic gold deposits is often underestimated, and independent mineralization systems may exist at depth." This gap severely constrains deep exploration breakthroughs in the mining area.

1.3. Research Objectives and Technical Approach

Addressing the above issues, this study proposes two core objectives:

1) Reveal the Critical Depth Effect: Quantitatively characterize the abrupt vertical changes in gold enrichment patterns through 3D modeling.

2) Decipher the Metallogenic Dynamics Process: Establish a spatio-temporal evolution model linking deep and shallow mineralization.

To achieve these goals, the innovative implicit geological modeling technique was introduced. Combined with variogram analysis and Kriging estimation, this approach enabled, for the first time, the decoupling of the mineralization structure at the full deposit scale (surface to −650 m). The scientific rationale of this technical route lies in: 3D models visually reflecting ore body geometry, while the grade coefficient of variation (CV value) effectively indicates the intensity of mineralization [14].

2. Data and Methods

2.1. Data Collection and Processing

Research data originates from mine production exploration, covering three main categories:

1) Geological Logging Data

Systematic collection and compilation of data from 220 underground drill holes and 523 stope samples (cumulative footage 38879.7 m) resulted in 2249 lithology identification points (Table 1(a) Logging data). Emphasis was placed on identifying host rocks and dikes: monzogranite, marble, silicified cataclasite, lamprophyre, quartz, and carbonate veins. Among these, pyrite-bearing carbonate veins, although volumetrically minor, were found in subsequent analysis to contribute significantly to the total gold metal endowment, hinting at their core role in mineralization.

2) Drill Hole Survey Data

In underground mine drilling, borehole deviation data is crucial. It directly impacts the precise location of target ore bodies or geological structures; correcting for spatial errors in ore body position caused by borehole deviation enhances the reliability of reserve calculations and geological models. All drilling in this study employed compass clinometers, with measurements of hole depth, azimuth, and inclination taken every 50 m. Stope and adit sampling used compass measurements, generating a deviation data table comprising 743 holes and 911 data points (Table 1(b) Locating data and Table 1(c) Survey data).

3) Sample Assay Data

This study utilized 18,415 samples (Table 1(d) Assay data), all assayed for Au grade by fire assay (detection limit 0.01 g/t). Data processing followed a three-step principle: First, outliers with analytical errors > 10% were eliminated; Second, extreme high grades (>60 g/t) were capped using the Top-cut method (threshold set at the 98th percentile); Third, the dataset was subdivided according to elevation gradient (10 m step interval) to provide input for 3D modeling.

Table 1. Data samples table.

(a) Logging data

Drillhole	No.	From	To	Lithology
ZK9-9-1	1	0	23.1	monzonitic granite
ZK9-9-1	2	23.1	64.2	marble
ZK9-9-1	3	64.2	77.3	monzonitic granite
ZK9-9-1	4	77.3	78.4	lamprophyre
ZK9-9-1	5	78.4	83.4	marble

(b) Locating data

Drillhole	X	Y	Z
ZK9-9-1	660523.277	126225.154	−9.00
ZK49-31-1	660251.221	125817.145	−49.00
ZK89-27-1	660415.600	125908.360	−89.00
ZK550-2-1	656065.013	125854.160	−550.00

Continued

(c) Survey data			
Drillhole	MD	Azim	Dev
ZK165-23-1	50.5	304	−0.2
ZK165-23-1	101.5	304	−2.2
ZK165-23-1	170.5	304	−3.7
ZK287-17-3	50.7	274	17.4
ZK287-17-3	80.7	274	15.7
(d) Assay data			
Drillhole	from	to	Au
ZK49-27-1	141.1	142.1	1.68
ZK49-27-1	142.1	143.1	29.7
ZK49-27-1	143.1	144.1	0.18
ZK49-27-1	144.1	145.1	0.34
ZK49-27-1	145.1	146	24.99

*Values shown are representative samples from the full dataset.

2.2. 3D Modeling

2.2.1. Lithological Model

Based on borehole lithology data, a 3D lithofacies framework (resolution 5 m*5 m*5 m) was built using a moving average interpolation algorithm. The advantage of this method is its ability to smooth the influence of local discrete points and accurately reproduce complex geological interfaces. The mathematical formula is:

$$\hat{Z}(x_0) = \frac{\sum_{i=1}^{n} \omega_i Z(x_i)}{\sum_{i=1}^{n} \omega_i}$$

$$\omega_i = \frac{1}{d(x_i, x_0)^k}$$

where ω_i is the weighting coefficient, $d(x_i, x_0)$ is the distance from the sample point to the estimation point, and k is an empirical value of 2.0. Modeling results clearly show: The marble-granite contact surface generally dips SE at ~123˚, with complex geometry. At shallow levels (<−400 m), granite intrusions penetrate marble layers, and marble also occurs as variably sized "xenoliths" within the granite. At depth (≥−400 m), the contact surface flattens, and large-scale silicified cataclasite zones appear (**Figure 2**).

2.2.2. Ore Body Modeling

Radial Basis Function (RBF, *Leapfrog Geo*) implicit modeling technology was applied to delineate mineralization domain boundaries (cut-off grade 0.8 g/t, representing the lower economic limit for this deposit). Key steps included:

Defining a signed distance field $\phi(x)$: Positive values inside the ore body, negative values in the wall rock. The interpolation function:

$$\phi(x)=\sum_{i=1}^{n}\lambda_i K\left(vertx-x_i vert\right)+P(x)$$

where $K(r)=r^3$ is the cubic spline kernel function; Generating a triangulated mesh model by extracting the isosurface using the Marching Cubes algorithm.

This method overcomes the subjectivity inherent in traditional manual interpretation and objectively reproduces the branching and merging characteristics of ore bodies (Figure 2).

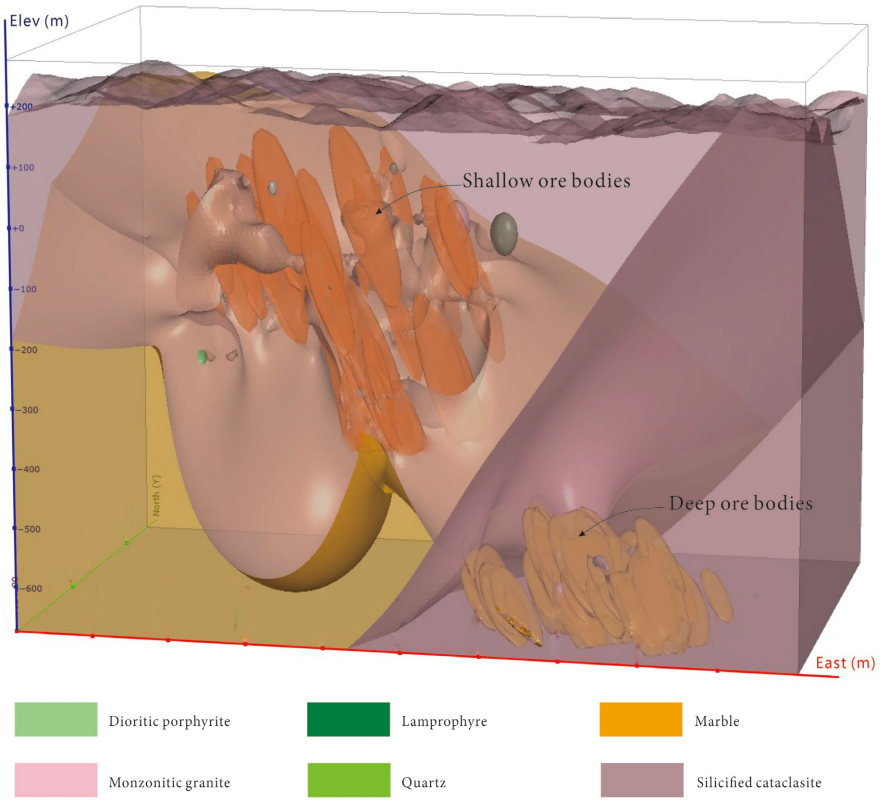

Figure 2. 3D geological model (illustrating lithologic contacts and differences in deep and shallow ore bodies characteristics).

2.2.3. Grade Spatial Estimation

Ordinary Kriging (OK) was employed for block estimation (grid size 5 m^3). The core task was fitting the optimal variogram model:

Shallow (<−400 m) spherical model:

$$\gamma(h)=C_0+C\left[\frac{3h}{2a}+\frac{1}{2}\left(\frac{h}{a}\right)^3\right],\quad C_0=0.25,\quad C=0.75,\ a=45\ m;$$

Deep (≥−400 m) exponential model:

$$\gamma(h)=C_0+C\left[1-\exp\left(-\frac{3h}{a}\right)\right],\quad C_0=0.15,\quad C=0.75,\ a=80\ m.$$

Model validation showed: Cross-validation average relative error was only 8.7%, confirming the reliability of the estimation results [15].

3. Analysis of 3D Enrichment Patterns

3.1. Spatial Structural Differentiation of Ore Bodies

The 3D model reveals a morphological discontinuity demarcated by the −400 m level (**Figure 2**). This differentiation is not a gradual transition but manifests as a distinct structural break:

Shallow Ore System (<−400 m):

Geometric Characteristics: Steeply dipping vein swarms (40˚ - 65˚), controlled by subsidiary NE-trending faults. Single veins extend ≤ 150 m, with an average thickness of 1.2 m. Adit and stope profiles show highly uneven pyrite alteration, confined to limited spaces (**Figure 3(a)**, **Figure 3(b)** showing limited thickness of shallow ore bodies strictly confined to contact zones).

Spatial Configuration: Veins are densely distributed within the granite-marble contact zone and fractures within the granite side (50 - 100 m), exhibiting a "main contact zone + feather fractures" pattern. High-grade cores (Au > 10 g/t) are strictly constrained by the contact zone.

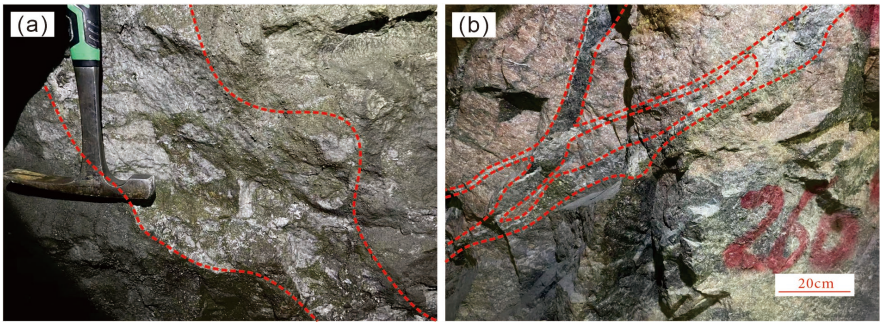

Figure 3. Distribution features of shallow ore bodies (illustrating schematic diagrams showing limited thickness of shallow ore bodies strictly confined to contact zones)

Deep Ore System (≥−400 m):

Geometric Characteristics: Gently dipping stratiform bodies (~20˚ - 30˚) distributed along the regional detachment fault, with continuous lengths > 230 m and an average thickness of 11.4 m. Drillhole core photographs illustrate the large scale of the ore bodies (**Figure 4**).

Spatial Configuration: The ore body footwall is planar or gently undulating, parallel to the detachment surface; the hanging wall is undulating or irregular, occurring within the cataclasite zone. Unlike the vein concentration in the shallow zone, gold minerals occur as disseminated grains within silicified altered rocks, with relatively uniform grade distribution.

This geometric leap reflects a shift in mineralization mechanisms-steep faults in the shallow zone favor open-space filling [16], while the deep detachment zone provides large-scale permeable pathways [13].

Figure 4. Representative drillhole core photographs from deep ore bodies (illustrating continuous and homogeneous mineralization with gold-bearing pyrite occurring in granular, vein, and disseminated forms within silicified granite).

3.2. Gold Grade Variability Patterns

The shallow domain grade frequency distribution shows significant positive skewness, with the mode shifted leftwards; grade values cluster in lower ranges but are still significantly higher than the deep domain, with multiple high-grade anomalies (>30 g/t). The coefficient of variation CV=1.52 (n = 10,212), indicating heterogeneous distribution. The semi-variogram shows a nugget effect of 0.25 (**Figure 5** Red curve), reflecting strong mineralization fluctuations at the micro-scale.

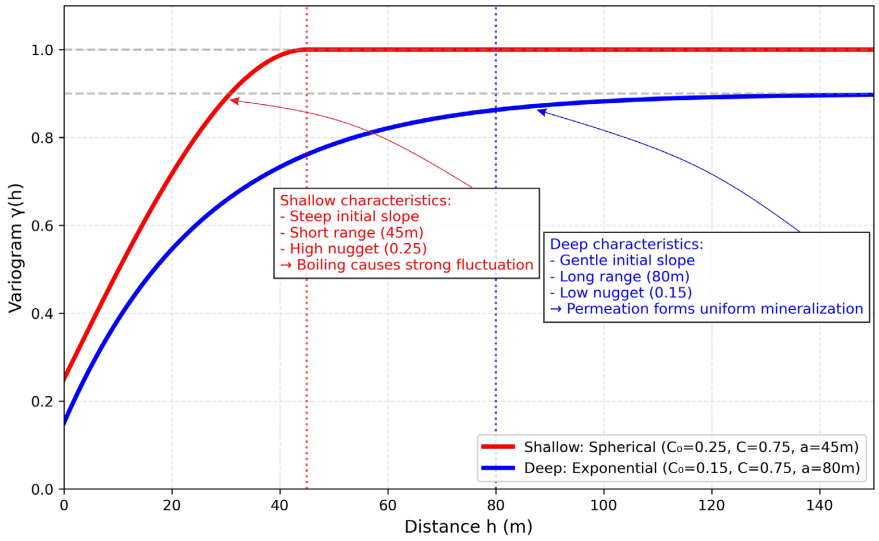

Figure 5. Variogram curve comparison: shallow vs deep orebodies.

This high variability is related to intermittent fracture filling caused by boiling. When ore-bearing fluids entered low-pressure zones, CO_2 loss caused a rapid pH increase, prompting the instantaneous decomposition of $Au(HS)_2^-$ complexes and precipitation of Au within dilatant fractures [17], forming visible native gold grains (**Figure 6**).

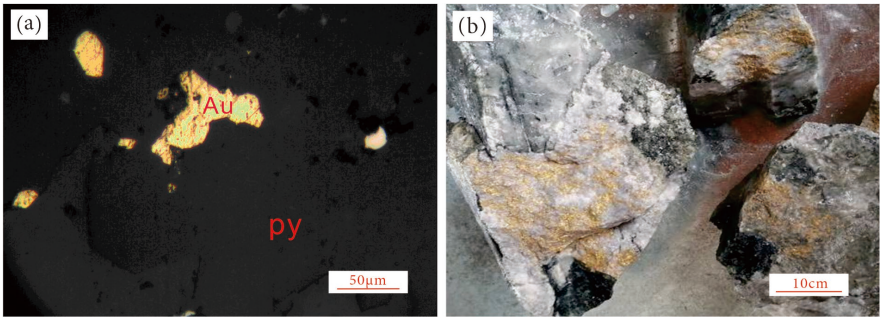

Figure 6. Shallow gold occurrence states. (a) Microscopic occurrence of Au—interstitial development between mineral crystals; (b) Visible gold.

The deep domain grade frequency distribution exhibits slight negative skewness, with overall grades significantly lower than the shallow domain. The coefficient of variation CV = 0.37 (n = 8203), indicating relative homogenization. The semi-variogram shows a nugget effect of only 0.15, with an extended range of 80 m (**Figure 5** Blue curve).

This low variability reflects a slow pervasive metasomatic process [18]. In the mesozonal environment at 280˚C - 320˚C, gold precipitated slowly as nano- to micro-sized particles within lattice defects of pyrite or mineral interstices, forming disseminated mineralization.

4. Integrated Deep-Shallow Metallogenic Analysis

Metallogenic Dynamic Process

Integrating the 3D geological model and spatial Au grade distribution characteristics with metallogenic dynamic analysis, this study proposes a two-stage evolutionary model:

Stage I: Deep-Seated Pervasive Alteration-Foundation (130 - 125 Ma, ≥−400 m)

Driving Mechanism: Early cretaceous crustal extension triggered anatectic magma emplacement (Zircon U-Pb age 130 ± 3 Ma [19]), releasing Au-As-S rich hydrothermal fluids.

Mineralization Process: Fluids migrated along the detachment zone. Under conditions of 280˚C - 320˚C, fluid-rock reactions occurred (e.g., $3Fe_2SiO_4 + 4H_2O \rightarrow Fe_3Si_2O_5(OH)_4 + Fe(OH)_2$), forming broad silicified zones. In this reducing environment, gold was transported as $Au(HS)_2^-$ and slowly precipitated via sulfidation: $2Au(HS)_2^- + Fe^{2+} \rightarrow 2Au^0 + 2H_2S + FeS_2$.

Product Characteristics: Formation of large-tonnage disseminated ore bodies, with gold occurring as nano- to micro-sized particles within pyrite or along min-

eral interstices (grain size < 10 μm).

Stage II: Shallow-Level Boiling Enrichment (122 - 118 Ma, <−400 m)

Triggering Factor: Continued extension caused brittle fracturing in the hanging wall of the detachment zone, forming a NE-trending fracture network [9].

Mineralization Process: Deep-seated fluids ascended along fractures to the lithostatic-hydrostatic pressure transition zone (ca. −400 m), where abrupt pressure drop triggered boiling (fluid inclusion vapor-liquid ratio abruptly increased to >40%). Boiling caused CO_2 loss, leading to a pH increase in the solution, destabilizing the $Au(HS)_2^-$ complex and causing decomposition [17]: $Au(HS)_2^- + ½H_2 \rightarrow Au^0 + 2HS^-$.

Product Characteristics: Rapid accumulation of pyrite-bearing carbonate veins within dilatant fractures.

5. Conclusions

1) 3D Modeling Confirms Vertical Zonation: The critical depth interface for the Liaoshang gold deposit is determined for the first time at −400 m. Above −400 m, the shallow zone develops NE-striking, steeply dipping, narrow, high-grade veins (avg. thickness 1.2 m, Au > 5.5 g/t), controlled by the monzogranite-marble belt. Below −400 m, gently dipping, stratiform low-grade ore bodies form (avg. thickness 18.4 m, Au = 2.1 ± 0.8 g/t), distributed along the basin-margin detachment fault. This dual geometric-grade discontinuity overturns the traditional concept of homogeneous mineralization.

2) Revealing the Essence of Synergistic Mineralization: Deep pervasive alteration and shallow boiling enrichment are continuous evolutionary products of the same hydrothermal system. The early stage (130 - 125 Ma) formed disseminated mineralization in a mesothermal reducing environment, contributing 68% of the resource. The late stage (122 - 118 Ma) generated vein-type enrichment in a lower-temperature oxidizing environment, locally increasing grades by 4 - 8 times.

3) Guiding Deep Exploration Breakthroughs: Through the 3D geological and grade models, significant resource potential below −600 m is revealed. Deep silicified cataclasite zones are prioritized targets for the next phase of exploration.

Acknowledgements

This research was supported by the Scientific Innovation Fund of Shandong No. 3 institute of geology and mineral exploration (Grant No. SYKJ-202303). Partial data were provided by Liaoshang gold mine, Shandong Humon smelting Co., Ltd. We gratefully acknowledge all contributions.

Conflicts of Interest

The authors declare no conflicts of interest.

References

[1] Zhai, M.G. (2022) Tectonic Evolution of the North China Craton. *Journal of Geo-*

mechanics, **25**, 722-745.

[2] Zhang, H., Sun, M., Zhou, X. and Ying, J. (2005) Geochemical Constraints on the Origin of Mesozoic Alkaline Intrusive Complexes from the North China Craton and Tectonic Implications. *Lithos*, **81**, 297-317. https://doi.org/10.1016/j.lithos.2004.12.015

[3] Yang, L., Deng, J., Zhang, L., Yang, W., Xie, D., Wang, L., *et al.* (2024) Jiaodong-Type Gold Deposit. *Acta Petrologica Sinica*, **40**, 1691-1711. https://doi.org/10.18654/1000-0569/2024.06.01

[4] Yang, L., Deng, J., Wang, Z., Guo, L., Li, R., Groves, D.I., *et al.* (2016) Relationships between Gold and Pyrite at the Xincheng Gold Deposit, Jiaodong Peninsula, China: Implications for Gold Source and Deposition in a Brittle Epizonal Environment. *Economic Geology*, **111**, 105-126. https://doi.org/10.2113/econgeo.111.1.105

[5] Wang, Z.X., Jiao, X.M., Ding, Z.J., Liu, X.M., Li, G.H., Ji, X.B. and Tang, J.Z. (2017) Structural Ore-Controlling Characteristics and Prospecting Direction of Liaoshang-Type Gold Deposit in the Northeastern Margin of Jiaolai Basin. *Gold Science and Technology*, No. 3, 61-69. https://doi.org/10.11872/j.issn.1005-2518.2017.03.061

[6] Li, Z.Q., Ding, Z.J., Bo, J.W., Wang, Z.X., Li, Y., Ji, P. and Li, T.T. (2024) Characteristics of Ore-Forming Fluids and Genesis of the Guocheng Gold Deposit in the Northeastern Margin of Jiaolai Basin. *Gold*, **45**, 57-63.

[7] Bo, J.W., Ding, Z.J., Song, M.C., Qiu, K.F., Sun, F.Y., Ji, P. and Zhang, R. (2021) C, O, S, Pb Isotopic Compositions and Genesis of the Liaoshang Gold Deposit in Jiaodong. *Acta Petrologica et Mineralogica*, **40**, 321-336.

[8] Zhang, L., Weinberg, R.F., Yang, L.Q., Groves, D.I. and Deng, J. (2020) Mesozoic Orogenic Gold Mineralization in the Jiaodong Peninsula, China: A Focused Event at 120 ± 2 Ma during Cooling of Pregold Granite Intrusions. *Economic Geology*, **115**, 415-441.

[9] Liang, H., Han, Z.Z., Wang, L.G., Tian, R.C., Wang, L.M., Wang, J.H., Zhi, Y.B., Zhang, W. and Liu, H.D. (2022) Fluid Inclusions, H-O-C-S-Pb Isotopic Characteristics and Genesis of the Liaoshang Gold Deposit in Jiaodong. *Geological Bulletin of China*, No. 6, 1053-1067.

[10] Shui, P. (2019) Geological Characteristics and Genetic Mechanism of the Guocheng-Liaoshang Gold Deposit in the Northeastern Margin of Jiaolai Basin. Master's Thesis, China University of Geosciences.

[11] Li, D.D. (2020) Study on the Genesis and Metallogenic Model of Longkou-Tudui Gold Mining Area in the Northeastern Margin of Jiaolai Basin. *Modern Mining*, No. 9, 6-11.

[12] Han, X.M., Duan, L.A., Zhao, P.F., Wang, J.T. and Guo, Y.C. (2024) Rb-Sr Isochron Age of Pyrite from the Qianchuiliu Gold Deposit in the Northeastern Margin of Jiaolai Basin, Shandong Province. *Geology in China*, No. 1, 366-367.

[13] Groves, D.I., Goldfarb, R.J., Gebre-Mariam, M., Hagemann, S.G. and Robert, F. (1998) Orogenic Gold Deposits: A Proposed Classification in the Context of Their Crustal Distribution and Relationship to Other Gold Deposit Types. *Ore Geology Reviews*, **13**, 7-27. https://doi.org/10.1016/s0169-1368(97)00012-7

[14] Abzalov, M.Z. (2006) Localised Uniform Conditioning (LUC): A New Approach for Direct Modelling of Small Blocks. *Mathematical Geology*, **38**, 393-411. https://doi.org/10.1007/s11004-005-9024-6

[15] Deutsch, C.V. and Journel, A.G. (1998) GSLIB: Geostatistical Software Library and User's Guide. 2nd Edition, Oxford University Press.

[16] Sibson, R.H. (1987) Earthquake Rupturing as a Mineralizing Agent. *Nature*, **327**, 142-144.

[17] Saunders, J.A. and Schoenly, P.A. (1995) Boiling, Colloid Nucleation and Aggregation, and the Genesis of Bonanza Au-Ag Ores of the Sleeper Deposit, Nevada. *Mineralium Deposita*, **30**, 199-210. https://doi.org/10.1007/bf00196356

[18] Yardley, B.W.D. and Cleverley, J.S. (2013) The Role of Metamorphic Fluids in the Formation of Ore Deposits. *Geological Society*, *London*, *Special Publications*, **393**, 117-134. https://doi.org/10.1144/sp393.5

[19] Fan, H., Hu, F., Yang, J. and Zhai, M. (2007) Fluid Evolution and Large-Scale Gold Metallogeny during Mesozoic Tectonic Transition in the Jiaodong Peninsula, Eastern China. *Geological Society*, *London*, *Special Publications*, **280**, 303-316. https://doi.org/10.1144/sp280.16